Effects of disorder on magnetic vortex gyration

Hongki Min[1,2],* R. D. McMichael[1], Jacques Miltat[1,2,3], and M. D. Stiles[1]

[1]*Center for Nanoscale Science and Technology, National Institute of*
Standards and Technology, Gaithersburg, Maryland 20899-6202, USA
[2]*Maryland NanoCenter, University of Maryland, College Park, Maryland 20742, USA*
[3]*Laboratoire de Physique des Solides, Université Paris Sud, CNRS, UMR 8502, F-91405 Orsay, France*

(Dated: February 16, 2011)

A vortex gyrating in a magnetic disk has two regimes of motion in the presence of disorder. At large gyration amplitudes, the vortex core moves quasi-freely through the disorder potential. As the amplitude decreases, the core can become pinned at a particular point in the potential and precess with a significantly increased frequency. In the pinned regime, the amplitude of the gyration decreases more rapidly than it does at larger precession amplitudes in the quasi-free regime. In part, this decreased decay time is due to an increase in the effective damping constant and in part due to geometric distortion of the vortex. A simple model with a single pinning potential illustrates these two contributions.

PACS numbers: 75.78.Fg, 75.70.Kw, 75.78.Cd

I. INTRODUCTION

In disks of magnetic material, the ground-state magnetic configuration is commonly a magnetic vortex state which forms due to the interplay between magnetostatic and exchange energies. In the vortex structure the magnetization in the wall curls around a vortex core and points out of the plane at the core region, as illustrated in Fig. 1. Alignment of the magnetization parallel to the edge of the disk minimizes the magnetostatic energy and the magnetization pointing out of the plane in the core avoids a singularity in the exchange energy. In the vortex state, the excitation spectrum is significantly modified compared to that of a uniform magnetization. In particular, there is a low-frequency gyration mode, in which the vortex core orbits around its minimum energy location.

The dynamics of a vortex state have been studied experimentally by time-resolved Kerr microscopy,[1–4] time-resolved scanning transmission x-ray microscopy,[5–7] and microwave reflection technique[8] and theoretically using a collective coordinate approach or micromagnetic simulations,[9–11] which show gyration frequencies typically in the subgigahertz range. If the vortex structure is excited strongly enough, the vortex core switches magnetization direction. Vortex core switching has been observed using time-resolved scanning transmission x-ray microscopy[12,13] and modeled using a collective coordinate approach or micromagnetic simulations.[14–17] These studies show a reversal of the vortex core magnetization with a relatively low threshold magnetic field on the order of milliteslas by an in-plane oscillating external magnetic field. Recent experiments have also studied vortex gyration and core reversal under excitation by current in the plane of the disk.[13,18–22] Excitation by current perpendicular to the disk has bee studied theoretically.[23–26] Current induced motion is beyond the scope of the present article.

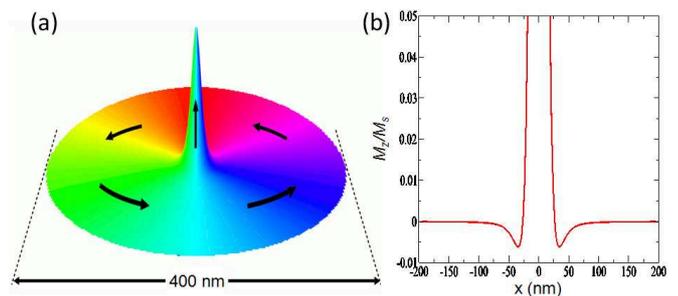Of particular interest here are experiments that measure the dynamics of vortices in disordered samples,[27]

FIG. 1: (Color online). (a) A typical vortex structure in a $Ni_{80}Fe_{20}$ disk with 400 nm diameter and 10 nm thickness calculated as described in Sec. II B. The color indicates the in-plane angle of the magnetization, and the arrows indicate the approximate magnetization direction. (b) Cross section of the z-component magnetization along the center of the vortex core in (a).

particularly the recent experiments by Compton *et al.*,[3,4] who measured vortex gyration in the presence of disorder. In these experiments, the vortex core is displaced by a static in-plane magnetic field and then a magnetic field pulse is applied to excite the vortex motion. At small magnetic-field-pulse amplitudes, the vortex gyrates about its equilibrium position with a frequency that is characteristic of the local disorder potential. At large pulse amplitudes, the vortex gyrates with a frequency determined by the magnetostatic energy of the disk. Between the two amplitudes, sharp transitions in the gyration frequency correspond to pinning or depinning of the vortex at local defects.

The collective coordinate approach mentioned above readily explains many aspects of these experiments.[3,4] Here, we address an aspect that has not yet been considered; that is, whether disorder changes the effective damping constant needed for a description of the behavior in terms of collective coordinates. This approach is motivated by our recent theoretical demonstration[28] that

when a magnetic domain wall propagates along a magnetic nanowire in the presence of disorder, the effective damping is enhanced as disorder increases, leading to increased or decreased domain wall velocity depending on the conditions. As a domain wall moves through disorder, internal degrees of freedom get excited, increasing the energy dissipation rate and thus the effective damping. The results of Compton *et al.* provide much more detailed information about the interaction of vortices with disorder than is typically accessible in experiments on domain wall motion in nanowires. This detail suggests that it might be possible to quantitatively connect theory and experiment relating enhanced damping.

In this article, we describe micromagnetic simulations of vortex gyration both in the complex case of random disorder and also in the simple case of a single pinning potential. Our results indicate that disorder, which exists inevitably in real experiments, affects the vortex dynamics in a way that can be interpreted as an enhancement of the effective damping. In Sec. II we describe the theoretical approach, in particular the micromagnetic simulations and the description of the dynamics in terms of a reduced set of degrees of freedom. In Sec. III we compare our simulations with the results of Ref. 3 and Ref. 4 showing the transition between quasi-free gyration and pinned gyration. In Sec. IV, we study this transition in a system with a single pinning potential to make clear the origin of various effects. Finally, in Sec. V, we discuss the implications of these results.

II. METHOD

A. Collective coordinate approach

Magnetization dynamics in a magnetic field can be described by the Landau-Lifshitz-Gilbert equation

$$\dot{\mathbf{M}} = \gamma \mathbf{H}_{\text{eff}} \times \mathbf{M} + \frac{\alpha_{\text{G}}}{M_{\text{s}}} \mathbf{M} \times \dot{\mathbf{M}}, \qquad (1)$$

where $\mathbf{H}_{\text{eff}}$ is the effective magnetic field including the external, exchange, demagnetization, and anisotropy fields; γ is the gyromagnetic ratio; M_{s} is the saturation magnetization; and α_{G} is the Gilbert damping constant. In the calculations described below, we study the dynamics of vortex gyration with Eq. (1) using a fixed value of α_{G}. We discuss an effective damping parameter α in the context of a description of the motion in terms of collective coordinates, which we describe next.

Vortex motion is frequently studied in models that adopt a description of vortex structures in terms of a limited number of collective coordinates.[29–33] For the simplest approximation, the vortex gyration is described by a two-dimensional vector $\mathbf{X} = (X_1, X_2)$ describing the vortex core position in a plane. Then Eq. (1) reduces to[29–33]

$$\alpha \mathbf{D} \dot{\mathbf{X}} = \mathbf{F} + \dot{\mathbf{X}} \times \mathbf{G}, \qquad (2)$$

where

$$D_{ij} = \frac{1}{M_{\text{s}}^2} \int dV \, \frac{\partial \mathbf{M}}{\partial X_i} \cdot \frac{\partial \mathbf{M}}{\partial X_j}, \qquad (3)$$

$$\mathbf{F} = \frac{\gamma}{M_{\text{s}}} \int dV \, \mathbf{H}_{\text{eff}} \cdot \frac{\partial \mathbf{M}}{\partial \mathbf{X}} = -\frac{\gamma}{\mu_0 M_{\text{s}}} \frac{\partial E}{\partial \mathbf{X}},$$

$$\mathbf{G} = \hat{\mathbf{z}} \frac{1}{M_{\text{s}}^3} \int dV \, \mathbf{M} \cdot \left(\frac{\partial \mathbf{M}}{\partial X_1} \times \frac{\partial \mathbf{M}}{\partial X_2} \right),$$

and E is a total energy functional whose derivative gives $\mu_0 \mathbf{H}_{\text{eff}} \equiv -\frac{\delta E}{\delta \mathbf{M}}$. Note that $\alpha \mathbf{D}$ is a symmetric matrix which characterizes viscous friction, $\mathbf{F}$ is a generalized force, and $\mathbf{G}$ is a gyrotropic tensor ($\dot{\mathbf{X}} \times \mathbf{G}$ is the gyrotropic force) which characterizes magnetization precession. Thus the dynamic properties of the vortex state are similar to that of a two-dimensional massless charged particle moving through a medium with a viscosity tensor $\alpha \mathbf{D}$ in the presence of an in-plane electric field $\mathbf{F}$ and a perpendicular magnetic field $\mathbf{G}$.[33] The "masslessness" of the dynamics is inherited from Eq. (1). In the absence of disorder, such a dynamics can be solved analytically by assuming harmonic oscillation for the vortex core.[9–11,34]

Assume that E has a quadratic dependence on the radial position of the vortex core r so that $\mathbf{F} = -kr\hat{\mathbf{r}}$, where k is a constant which characterizes the shape of the potential in which the vortex core gyrates. In polar coordinates, Eq. (2) can be expressed in the following matrix form

$$\alpha \begin{pmatrix} D_{rr} & D_{r\phi} \\ D_{r\phi} & D_{\phi\phi} \end{pmatrix} \begin{pmatrix} \dot{r} \\ r\dot{\phi} \end{pmatrix} = \begin{pmatrix} -kr + Gr\dot{\phi} \\ -G\dot{r} \end{pmatrix}, \quad (4)$$

where ϕ is the azimuthal angle of the vortex core position from the gyration center.

Assuming $r = r_0 \exp(-t/\tau)$ and $\phi = 2\pi f t$, and by eliminating k, we have

$$2\pi f \tau C \alpha = 1, \qquad (5)$$

where $C = D_{\phi\phi}/(G + \alpha D_{R\phi})$. These four parameters, the gyration frequency f, the decay time τ, the effective damping parameter α, and the geometrical factor C, are the focus of the subsequent analysis. A related analysis was carried out by Compton *et al.*[3,4] to model behavior of the precession frequency f in the presence of a pinning potential. They assumed that D and G were constant. Here, we focus on the decay time, τ, which is also measurable and examine the extent it is modified by changes in D, G, and the effective damping, α. The geometrical factor C is related to the deformation of a vortex structure, which is hard to measure but can be evaluated in a simulation using Eq. (3). In analyzing measurements of the decay time, it would be tempting to assume that C is constant and ascribe the observed changes in $f\tau$ as due to changes in α. Here, we test the degree to which that would be correct. Note that Eq. (5) is explicitly independent of k, thus independent of a specific potential shape in which a vortex gyrates. However, each of the parameters in Eq. (5) depends on k. In particular C depends

on the vortex shape, and hence does depend weakly on k for the disks of interest here.

Now imagine a vortex gyration experiment in a disk with a pinning potential at the center. When a large enough field pulse is applied, a vortex gyrates outside of the pinning potential and as the orbit decays, it is eventually trapped by the potential. The frequency of the precession f and its decay time τ change when the vortex becomes pinned

$$\frac{f_0 \tau_0}{f \tau} = \frac{\alpha_{\mathrm{eff}}}{\alpha_0} \frac{C}{C_0}, \qquad (6)$$

where α_{eff}, f, τ, and C indicate values in the trapped region while those with the subscript 0 indicate values in free region. The frequency and decay time can be measured so if the vortex geometry stays the same, that is if C remains constant, measurements of f and τ could be used to infer the change in the effective damping constant. In Sec. IV, however, we will show that C is not constant in the presence of disorder.

When the motion of the vortex is well described by the collective coordinates, we expect that $\alpha_{\mathrm{eff}} = \alpha_0 = \alpha_{\mathrm{G}}$. However, if other modes of the system are excited, the total energy dissipation rate would increase leading to an increase in the effective values of α and faster decay (smaller τ). One of the goals of this work is to characterize this increase and to compare it to the increase observed in the modeled motion of vortex domain walls.[28] In the subsequent sections, we use micromagnetic simulations to study how the effective damping is changed during the gyration motion and how it affects the decay time of the gyration. We stress that the "real" damping constant does not change, but the value consistent with the collective coordinate description does.

B. Micromagnetic simulation

We compute the dynamics of the vortex state through numerical solution of Eq. (1) using the Object Oriented MicroMagnetic Framework (OOMMF).[35] We set up a $\mathrm{Ni}_{80}\mathrm{Fe}_{20}$ disk with a 400 nm diameter and a 10 nm thickness, as shown in Fig. 1(a). We use computational cells that are uniform through the thickness and have an in-plane size of 2.5 nm. For material constants, we use the saturation magnetization $M_{\mathrm{s}}=800$ kA/m, damping constant $\alpha_{\mathrm{G}}=0.01$ and either a fixed value of the exchange stiffness constant $A=13$ pJ/m or the exchange length $l_{\mathrm{ex}} = 5.7$ nm. Note that

$$l_{\mathrm{ex}} \equiv \left[2A/(\mu_0 M_{\mathrm{s}}^2) \right]^{1/2}. \qquad (7)$$

We tested the cell size dependence by studying a system with reduced size – 200 nm diameter and 5 nm thickness – and compared the results of simulations with cell sizes 1.25 nm and 2.5 nm. We found that these simulations agree to within 5 % with no qualitative differences. Thus, for the bigger system we treat in this article, with
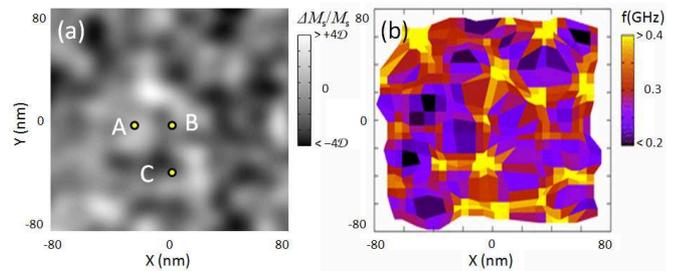

FIG. 2: (Color online). (a) A typical disorder image with 10 nm spatial correlation length, and (b) contour maps of the gyration frequency as a function of position. (a) Part of the saturation magnetization within a $\mathrm{Ni}_{80}\mathrm{Fe}_{20}$ disk with a 400 nm diameter and a 10 nm thickness. White indicates maxima in the magnetization and black minima. These results are based on a model of the disorder with $\mathcal{D} = 0.05$ and a fixed exchange stiffness constant A. (b) The gyration frequency according to the color scale on the right. To move the vortex positions, in-plane static magnetic fields from -10 mT to $+10$ mT along the x and y directions were applied. The gyration frequency is obtained by applying a field pulse of 0.1 mT for 200 ps along the y direction. The final location of the vortex core determines the real space position used in the figure.

400 nm diameter and 10 nm thickness, we use a 2.5 nm cell size.

C. Disorder model

We motivate our model for disorder on the measurements in Ref. 3. The article shows magnetic force microscopy images that reveal thickness fluctuations with a characteristic length scale of about 10 nm. Rather than dealing with a full-fledged model of thickness fluctuations, we introduce disorder by varying the saturation magnetization M_{s} while fixing either A or l_{ex}. In the main text, we fix A and, in the Appendix, we discuss the quantitative but not qualitative changes that occur when we fix l_{ex}. We generate a random, white-noise model for the variation of M_{s} and convolute it with a Gaussian that has a width of 10 nm. A typical disorder image is shown in Fig. 2(a), showing the smooth variation of M_{s} guaranteed by the convolution. Regions with reduced magnetization, intended to model thin parts of the sample, are shown in black and tend to create pinning centers for the vortex core and locally increase the gyration frequency as shown in Fig. 2(b).

To estimate realistic disorder amplitudes, we compute the variation of the gyration frequencies to be compared with the measurements in Ref. 3, which show a factor of 2 to 3 variation in resonance frequency as a vortex is scanned over a disk-shaped sample. We compute the precession frequency in the limit of low precession amplitudes as a function of H_x and H_y, in correspondence with the experimental procedure. In distinction to the experiment, we can view the equilibrium position of the
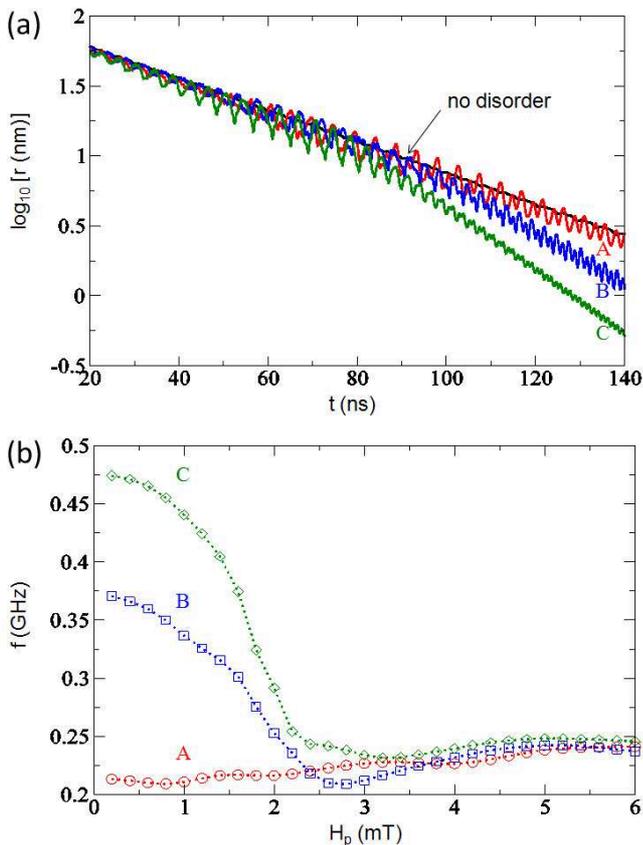
FIG. 3: (Color online). (a) Time evolution of gyration radius r for the disordered sample in Fig. 2 at points A, B and C for $\mathcal{D} = 0.05$ with fixed A. To excite a vortex state, a Gaussian-type field pulse of 20 mT with 1 ns of the full width at half maximum along the y direction is applied. The black line is for the case without disorder. The small amplitude oscillations are due to the excitation procedure, which does not produce purely circular precession. (b) The gyration frequency averaged from $t = 2$ ns to 12 ns as a function of field pulse amplitude at the points A, B and C.

vortex in real space and plot the frequency as a function of position to see the correlations with the disorder image. The mapping from applied field to vortex position is responsible for the irregular grid seen in Fig. 2(b). For these calculations, we characterize the size of the disorder by the ratio of the standard deviation of the fluctuations in the <u>magnetization</u> to the saturation magnetization, $\mathcal{D} = \sqrt{\langle (M(\mathbf{r}) - M_{\mathrm{s}})^2 \rangle}/M_{\mathrm{s}}$. We limit the size of the fluctuations to ensure that the magnetization stays positive. We find that for a fixed A, a disorder value of $\mathcal{D} = 0.05$ gives roughly the same gyration frequency variation as the experiment. The modeled frequency variation is shown in Fig. 2(b).

III. VORTEX GYRATION IN A DISORDERED FILM

First, we study the dynamics of vortex gyration in the disordered sample shown in Fig. 2 for $\mathcal{D} = 0.05$ with fixed A. To move a vortex core to different positions, we apply in-plane static magnetic fields to the sample. Maintaining the static in-plane magnetic fields, we apply an additional Gaussian-type field pulse of 20 mT along the y direction with a 1 ns full width at half maximum to excite the gyration motion. This pulse is large enough to induce a free vortex gyration with an initial radius that is much larger than the disorder correlation length. The gyration radius decreases with time because of the energy dissipation through damping, and eventually the vortex is trapped by the disorder potential when its gyration radius is approximately the correlation length of the disorder potential, which is 10 nm in the simulations.

Figure 3 shows the behavior of the gyration for vortex center positions, A, B and C in Fig. 2. Position A is in a relatively flat region of the disorder potential, position C is close to a minimum in the disorder potential, and position B is intermediate between the two. Figure 3(a) shows the time evolution of the gyration radius r. For "free" precession, before the vortex becomes trapped, the gyration frequency and decay rate are almost the same as the corresponding quantities in a disk without disorder, and the vortex gyration motion is not changed significantly by the disorder potential. As we discuss in Sec. V, these results indicate that gyration in the "free" regime is minimally affected by disorder and there does not appear to be an increase in the effective damping parameter in this regime. This result is in stark contrast to the behavior found for the motion of a vortex domain wall through a disorder potential. This contrast will be discussed in more detail in Sec. V. In the trapped regime, after approximately 90 ns, the decay rate of the precession radius increases dramatically for positions B and C, those points close to minima in the disorder potential. This change in decay rate is associated with changes in the precession rate.

Figure 3(b) shows the change of the gyration frequency as the field-pulse amplitude is varied, by averaging over a fixed interval (from $t = 2$ ns to 12 ns) after the pulse. At small field-pulse amplitudes, the vortex gyrates about its equilibrium position at points A, B and C with a frequency characteristic of each pining site. At large pulse amplitudes, the vortex core is depinned and gyrates with the frequency of the free region. Between the two amplitudes, as a function of field pulse amplitude, there is a crossover above which the gyration frequency drops to the value of the free region due to depinning of the vortex core from the pinning site. Here, the transition is gradual because, for some fields, the vortex core does not completely escape the pinning potential and may even, for slightly higher fields, become repinned during the averaging interval. A related measurement in Ref. 4 shows much more abrupt transitions in Fig. 10(b). However,

there are significant differences in the excitation pulse shape that strongly affect transition width as illustrated in Fig. 10(d) in that same article. Note that the crossover field here is a field range corresponding to the vortex completely escaping the pinning potential without being trapped again for a fixed time interval. For a Gaussian field pulse with a 1 ns full width at half maximum, the crossover field for the time average between 2 ns and 12 ns is approximately 2 mT for points B and C.

IV.   GYRATION IN A SINGLE PINNING POTENTIAL

A.   Numerical results

The existence of two regimes of motion of a vortex in a disordered disk suggests that the behavior should be captured by a simple model of a single pinning potential in the center of an otherwise ideal disk. Extreme examples of such samples, in which a hole has been fabricated in the disk have been studied experimentally[27,36] and theoretically.[34] Theoretical studies in Ref. 4 are similar to ours but focus on changes in the gyration frequency. We choose the radius of the single pinning potential to be $r_{\mathrm{pin}} = 10$ nm as a typical length scale of the potential. Inside the potential, the magnetization increases quadratically from the center. We characterize the potential depth as the ratio of reduced magnetization at the center ΔM_{c} to the saturation magnetization M_{s}, $\delta = \Delta M_{\mathrm{c}}/M_{\mathrm{s}}$. The vortex gyration is excited by a Gaussian-type field pulse along the y direction of 20 mT with a 1 ns full width at half maximum. When the strength of the field pulse is large enough, the vortex core gyrates outside of the pinning potential with a frequency that is determined by the geometry of the disk. The radius of the gyration decreases due to the energy dissipation through damping. When the vortex core enters the pinning potential, it is trapped by the potential and the gyration frequency changes.

Figure 4 shows the time evolution of the gyration radius r, the gyration frequency f, and the deformation factor C for depth ratios $\delta = 0, 0.1, 0.2, 0.3$ and 0.4 with fixed A. Here f is obtained from the angular velocity of gyration motion and C is calculated from Eq. (3). From the slope of the logarithm of r we can obtain the decay time τ. When the gyration radius becomes close to 10 nm, which is the radius of the pinning potential, τ, f, and C change, indicating that the vortex has become trapped by the pinning potential. As δ increases, τ and C decrease while f increases in the trapped regime. Note that additional oscillations superimposed on the curves have a frequency of twice the gyration frequency and originate because the short pulse with which we excite the gyration leads to a slightly elliptical orbit for the vortex core.

Figure 5 shows the evolution of the different factors in Eq. (6) as the depth of the pinning potential is varied.
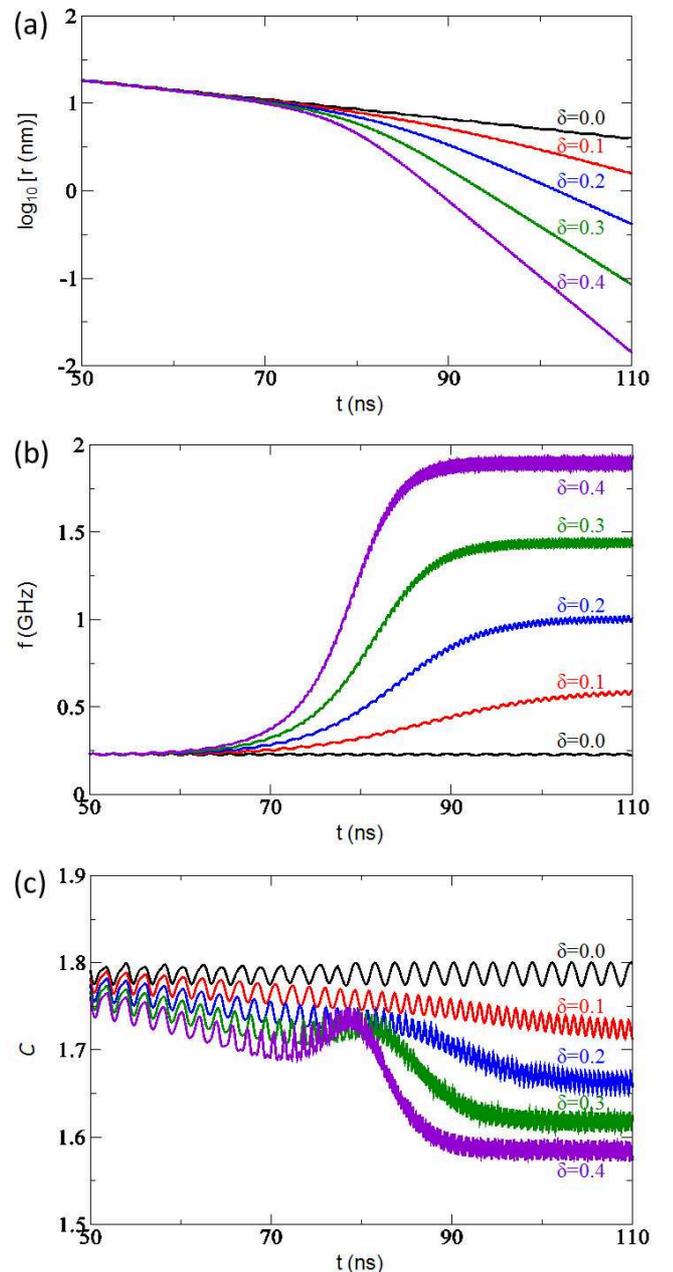

FIG. 4: (Color online). Time evolution of (a) gyration radius r, (b) gyration frequency f and (c) deformation factor C in a single pinning potential of the radius 10 nm for the depth ratio $\delta = 0, 0.1, 0.2, 0.3$ and 0.4 with fixed A. The gyration is excited by a 1 ns pulse of 20 mT.

Since f and τ can be measured experimentally, for example, from the Kerr microscopy analysis, it is tempting to attribute the change in the decay to the change in the effective damping. However, Fig. 5 shows that, in fact, most of the change is due to a change in the geometry of the vortex through the factor C, which can be extracted from the simulations. In fact, ignoring the changes in C would lead to the erroneous conclusion that damping
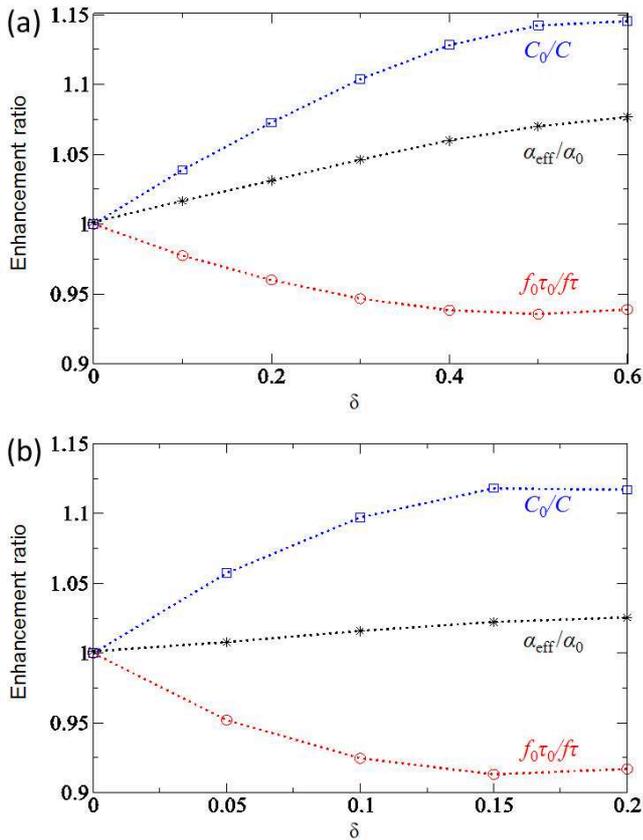
FIG. 5: (Color online). Enhancement ratio of $f\tau$, C, and α_{eff} as a function of depth ratio δ for (a) fixed A and (b) fixed l_{ex}. Subscript 0 indicates values in the free region before trapping.

decreases as the depth of the well increases for the case considered here. The actual values of the enhancement rate depend on various factors such as the type of disorder, geometry of samples, and material properties such as the saturation magnetization and the exchange constant.

B.   Radius dependence of the effective damping

Figure 6 shows the frequency dependence of the effective damping for the different radii of the pinning potential r_{pin} with fixed A. As the frequency increases, the vortex gets more excited increasing the effective damping. Note that its slope increases as the radius of the pinning potential increases and then saturates around $r_{\text{pin}} \approx 60$ nm, which is approximately the distance from the center of a disk to the point where the z component becomes zero, as shown in Fig. 1(b).

V.   DISCUSSION

Disorder in magnetic samples can increase the energy dissipation rate both for vortex gyration and domain wall
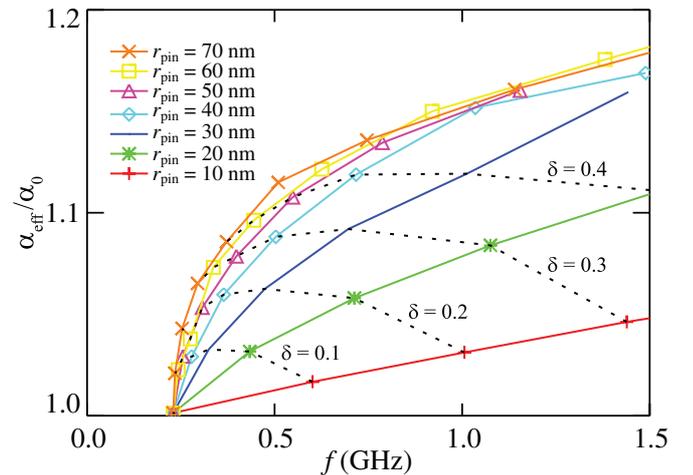

FIG. 6: (Color online). Frequency dependence of the effective damping for fixed A and various pinning potential radii $r_{\text{pin}} = 10$ nm, 20 nm, ... 70 nm and depth ratios $\delta = 0, 0.1, 0.2, 0.3, 0.4$. Solid lines indicate values for constant r_{pin} and dashed lines constant δ.

propagation as shown earlier.[28] An important contribution to this appears to occur when the motion through the disorder excites additional degrees of freedom in addition to the overall motion. We refer to these degrees of freedom as internal. If these internal degrees of freedom are not included explicitly in a collective coordinate model,[33] they will typically lead to an increase in the effective damping parameter that describes the motion. Vortex gyration appears to give much smaller increase in the effective damping than is found for domain wall motion[28] but may be more accessible experimentally.[3,4]

The modeling results described in this article agree with the recent experiments and theoretical analysis in Refs. 3 and 4, demonstrating the frequency changes between the free and trapped regimes. Perhaps not surprisingly, the transition between high-amplitude and low-amplitude occurs when the gyration radius is comparable to the correlation length. Here, we focus not on the change of the frequencies between the two regimes, but on the change of the effective damping constant, which is much smaller than that of the frequency.

Disorder has a negligible effect on the gyration decay rate when the gyration amplitude is large. However, the decay rate is increased by disorder when gyration amplitude is small. While a naive interpretation would attribute changes in the product of gyration frequency and decay time $f\tau$ to changes in the effective damping parameter α, a more detailed interpretation in the context of the collective coordinate approach shows that the majority of the change in $f\tau$ is due to disorder-induced changes in the deformation factor C, and that the change in α is modest. Even though the change in the frequency can be successfully modeled assuming the deformation factor C is constant, evaluating the effective damping correctly

requires detailed calculation.

Comparing these vortex gyration results with the results of similar calculations on vortex wall propagation, it is clear that the domain wall motion is more sensitive to disorder. For field or current induced vortex wall propagation in the presence of M_s fluctuations with fixed A,[28] the effective damping is enhanced almost two times for $\mathcal{D} = 0.05$ (5 % average fluctuation of M_s). For vortex gyration in a single pinning potential with fixed A, however, the damping is enhanced by only 6 % even for $\delta = 0.4$ (40 % of reduced magnetization at the center), as shown in Fig. 5.

One possible reason for this difference is the appearance of half antivortices in domain wall propagation. As the vortex wall propagates either by field or current along a magnetic nanowire, energy dissipates mostly through the motion of the vortex core and two half antivortices.[28] The relative motions of these structures are examples of internal degrees of freedom. When these are excited by moving in the disorder potential, the energy dissipation rate increases. In a disk, on the other hand, there are no antivortices, as seen in Fig. 1. When vortices are driven to large amplitudes, antivortices can appear and can lead to core reversal[14] when the system is driven hard enough. In the simulations we consider here, we are not in this regime and the distortions of the vortex are relatively small. The lack of antivortices in these simulations is consistent with a reduced excitation of internal degrees of freedom as compared to the vortex wall propagation, resulting in the smaller enhanced effective damping.

In summary, we have demonstrated that disorder enhances the effective damping, and the enhancement ratio can be estimated up to the deformation factor by a vortex gyration experiment in a magnetic disk with a single pinning potential at the center. By measuring the frequency f and decay time τ in free and trapped regions, we can estimate the enhancement ratio of the effective damping times the deformation factor.

Appendix: Fixed A vs fixed l_{ex}

In this article we are using a simple approximation to model the effect of thickness fluctuations. Since the important energies in the problem are the magnetostatic (stray field) energy, the Zeeman energy, and the exchange energy, we can capture the changes in the first two by locally varying the saturation magnetization M_s. In the main body of the text, we report results for vortex gyration as we model thickness variations by changing M_s

while keeping the exchange constant A constant. An alternate approach would be to keep the exchange length $l_{ex} = [2A/(\mu_0 M_s^2)]^{1/2}$ constant. In this appendix, we describe the quantitative but not qualitative changes that result.

For a fixed l_{ex}, a disorder value of $\mathcal{D} = 0.0125$ gives a similar variation in gyration frequency as a value of $\mathcal{D} = 0.05$ for constant A. We attribute the higher sensitivity to disorder with fixed l_{ex} to changes in exchange energy in the region outside the vortex core. Briefly, Eq. (7) shows that A becomes a function of M_s when l_{ex} is fixed. Consequently, the exchange energy associated with the curling of the magnetization around the vortex core decreases when M_s decreases.

For a single pinning potential, simulations for the fixed l_{ex} case show similar trends as seen in Fig. 4 but with larger frequency and smaller decay time compared with the fixed A case. In addition, we see in Fig. 5(b) that the fixed l_{ex} case leads to a smaller change in the effective damping for a given change in $f\tau$ as compared to the fixed A case.

To understand the difference between M_s fluctuations with fixed A and those with fixed l_{ex}, consider a simple model of a vortex in a thin film disk with thickness z. We estimate the core energy and how it varies with the reduction in the magnetization in the pinning potential for both fixed A and fixed l_{ex}. We model the pinning potential as a circular region of radius r_{pin} of uniformly reduced magnetization M_{pin}. We assume that the vortex can be described as a core region within a radius r_c where the magnetization points out of plane, and an outer region $r > r_c$ where the magnetization is directed azimuthally. Our approach is to estimate the change in vortex energy as M_{pin} is varied in the pinning potential region , $r < r_{pin}$. For simplicity, we just consider the case for $r_c < r_{pin}$.

In the core region, the magnetization is uniform, and the energy density is magnetostatic, thus we can approximate the energy of the core as

$$E_{core} = \pi r_c^2 z \frac{1}{2} \mu_0 M_{pin}^2. \qquad (A.1)$$

In this expression we have assumed that $z \ll r_c$ for simplicity.

The divergence of the magnetization in the outside region, $r > r_c$, is zero and the magnetization is perpendicular to the stray fields from the core region, so the energy in the outside region is entirely exchange energy. Since the magnetization outside r_{pin} does not depend on M_{pin} and the geometry of the vortex is fixed (exactly in this simple model and approximately in a full simulation), the energy of the magnetization from r_{pin} out to R, the radius of the disk, does not change. Ignoring that constant contribution leaves the M_{pin}-dependent change

in the exchange energy from r_c to r_{pin}

$$E_{outside} = \int dv \frac{A}{M_{pin}^2} \left(\frac{d\mathbf{M}}{d\mathbf{x}} \right)^2$$
$$= 2\pi z A \ln(r_{pin}/r_c). \qquad (A.2)$$

As a further approximation, we ignore any exchange energy associated with the sharp transition from vertical to in-plane magnetization at the core boundary, r_c.

So far, the core radius has been left as a variable, and we determine its value by minimizing the total energy $E_{total} = E_{core} + E_{outside}$. The result is

$$r_{c,min} = \sqrt{\frac{2A}{\mu_0 M_{pin}^2}} \equiv l_{ex}, \qquad (A.3)$$

and the minimized energy is

$$E_{total} = \pi z A \left[1 + \ln \left(\frac{r_{pin}^2 \mu_0 M_{pin}^2}{2A} \right) \right] \qquad (A.4)$$

or equivalently,

$$E_{total} = \pi l_{ex}^2 z \frac{1}{2} \mu_0 M_{pin}^2 \left[1 + 2\ln \left(\frac{r_{pin}}{l_{ex}} \right) \right]. \qquad (A.5)$$

Therefore, from Eqs. (A.4) and (A.5), the ratio of the total energy changes using constant A compared to constant l_{ex} is

$$\frac{\left. \frac{dE_{total}}{dM_{pin}} \right|_{l_{ex}}}{\left. \frac{dE_{total}}{dM_{pin}} \right|_A} = 1 + 2\ln \left(\frac{r_{pin}}{l_{ex}} \right). \qquad (A.6)$$

For $r_{pin} = 10$ nm and $l_{ex} = 5.7$ nm, the ratio is ≈ 2.1. That is, the energy is more sensitive to variations in M_{pin} for fixed l_{ex} than for fixed A.

With A fixed, a decrease in M_{pin} results in an expansion of the core radius [see Eq. (A.3)] such that the decreased magnetostatic energy density within the core is compensated by an increased core volume, yielding no net change in the magnetostatic energy. The net energy change is due to a decrease in the exchange energy as the region $r_c < r < r_{pin}$ becomes smaller as r_c increases.

In contrast, for fixed l_{ex}, the geometry of the core is fixed, and there is a decrease in the magnetostatic energy of the core associated with a decrease in M_{pin}. Further, with l_{ex} fixed it can be seen from (A.3) that A must decrease with M_{pin}, and this results in reduced exchange energy calculated in the region $r_c < r < r_{pin}$.

* Electronic address: hmin@umd.edu; Current address: Condensed Matter Theory Center, Department of Physics, University of Maryland, College Park, Maryland 20742, USA

[1] J. P. Park, P. Eames, D. M. Engebretson, J. Berezovsky, and P. A. Crowell, Phys. Rev. B **67**, 020403(R) (2003).

[2] Xiaobin Zhu, Zhigang Liu, Vitali Metlushko, Peter Grütter, and Mark R. Freeman, Phys. Rev. B **71**, 180408(R) (2005).

[3] R. L. Compton and P. A. Crowell, Phys. Rev. Lett. **97**, 137202 (2006).

[4] R. L. Compton, T. Y. Chen, and P. A. Crowell, Phys. Rev. B **81**, 144412 (2010).

[5] S.-B. Choe, Y. Acremann, A. Scholl, A. Bauer, A. Doran, J. Stöhr, and H. A. Padmore, Science **304**, 420 (2004).

[6] K. Kuepper, L. Bischoff, Ch. Akhmadaliev, J. Fassbender, H. Stoll, K. W. Chou, A. Puzic, K. Fauth, D. Dolgos, G. Schütz, B. Van Waeyenberge, T. Tyliszczak, I. Neudecker, G. Woltersdorf, and C. H. Back, Appl. Phys. Lett. **90**, 062506 (2007).

[7] A. Vansteenkiste, J. De Baerdemaeker, K. W. Chou, H. Stoll, M. Curcic, T. Tyliszczak, G. Woltersdorf, C. H. Back, G. Schütz, and B. Van Waeyenberge, Phys. Rev. B **77**, 144420 (2008).

[8] V. Novosad, F. Y. Fradin, P. E. Roy, K. S. Buchanan, K. Yu. Guslienko, and S. D. Bader, Phys. Rev. B **72**, 024455 (2005).

[9] K. Yu. Guslienko, B. A. Ivanov, V. Novosad, Y. Otani, H. Shima, and K. Fukamichi, J. Appl. Phys. **91**, 8037 (2002).

[10] K. Yu. Guslienko, W. Scholz, R. W. Chantrell, and V. Novosad, Phys. Rev. B **71**, 144407 (2005).

[11] K. Yu. Guslienko, Appl. Phys. Lett. **89**, 022510 (2006).

[12] B. Van Waeyenberge, A. Puzic, H. Stoll, K. W. Chou, T. Tyliszczak, R. Hertel, M. Fähnle, H. Brückl, K. Rott, G. Reiss, I. Neudecker, D. Weiss, C. H. Back, and G. Schütz, Nature 444, **461** (2006).

[13] A. Vansteenkiste, K. W. Chou, M. Weigand, M. Curcic, V. Sackmann, H. Stoll, T. Tyliszczak, G. Woltersdorf, C. H. Back, G. Schütz, and B. Van Waeyenberge, Nature Physics **5**, 332 (2009).

[14] K. Yu. Guslienko, K.-S. Lee, and S.-K. Kim, Phys. Rev. Lett. **100**, 027203 (2008).

[15] A Vansteenkiste *et al.*, New J. Phys. **11** 063006 (2009).

[16] F. A. Apolonio, W. A. Moura-Melo, F. P. Crisafuli, A. R. Pereira, and R. L. Silva, J. Appl. Phys. **106**, 084320 (2009).

[17] R. L. Silva, A. R. Pereira, R. C. Silva, W. A. Moura-Melo, N. M. Oliveira-Neto, S. A. Leonel, and P. Z. Coura, Phys. Rev. B **78**, 054423 (2008).

[18] S. Kasai, Y. Nakatani, K. Kobayashi, H. Kohno, and T. Ono, Phys. Rev. Lett. **97**, 107204 (2006).

[19] K. Yamada, S. Kasai, Y. Nakatani, K. Kobayashi, H. Kohno, A. Thiaville, and T. Ono, Nat. Mater. **6**, 269 (2007)

[20] R. Hertel, S. Gliga, M. Fähnle, and C. M. Schneider, Phys. Rev. Lett. **98**, 117201 (2007).

[21] V. S. Pribiag, I. N. Krivorotov, G. D. Fuchs, P. M. Braganca, O. Ozatay, J. C. Sankey, D. C. Ralph, and R. A. Buhrman, Nat. Phys. **3**, 498 (2007).

[22] V. S. Pribiag, G. Finocchio, B. J. Williams, D. C. Ralph, and R. A. Buhrman, Phys. Rev. B **80**, 180411(R) (2009).

[23] J.-G. Caputo, Y. Gaididei, F. G. Mertens, and D. D. Sheka, Phys. Rev. Lett **98**, 056604 (2007).

[24] D. D. Sheka, Y. Gaididei, and F. G. Mertens, Appl. Phys. Lett. **91**, 082509 (2007).

[25] Y. Gaididei, V. P. Kravchuk and D. D. Sheka Int. J. of Quant. Chem., **110**, 83 (2010).

[26] K. Y. Guslienko, R. H. Heredero, and O. Chubykalo-Fesenko, Phys. Rev.B, **82**, 014402 (2010).

[27] T. Uhlig, M. Rahm, C. Dietrich, R. Höllinger, M. Heumann, D. Weiss, and J. Zweck, Phys. Rev. Lett. **95**, 237205 (2005).

[28] H. Min, R. D. McMichael, M. J. Donahue, J. Miltat, and M. D. Stiles, Phys. Rev. Lett. **104**, 217201 (2010).

[29] A. A. Thiele, Phys. Rev. Lett. **30**, 230 (1973).

[30] A. Thiaville, Y. Nakatani, J. Miltat, and Y. Suzuki, Europhys. Lett. **69**, 990 (2005).

[31] J. He, Z. Li, and S. Zhang Phys. Rev. B **73**, 184408 (2006).

[32] O. A. Tretiakov, D. Clarke, Gia-Wei Chern, Ya. B. Bazaliy, and O. Tchernyshyov, Phys. Rev. Lett. **100**, 127204 (2008).

[33] D. J. Clarke, O. A. Tretiakov, G.-W. Chern, Ya. B. Bazaliy, and O. Tchernyshyov, Phys. Rev. B **78**, 134412 (2008).

[34] G. M. Wysin, J. Phys. Condens. Matt. 22, 376002 (2010).

[35] M. J. Donahue and D. G. Porter, Interagency Report NISTIR 6376, National Institute of Standards and Technology, Gaithersburg, MD (Sept. 1999), http://math.nist.gov/oommf/.

[36] F. Hoffmann, G. Woltersdorf, K. Perzlmaier, A. N. Slavin, V. S. Tiberkevich, A. Bischof, D. Weiss, and C. H. Back, Phys. Rev. B **76**, 014416 (2007).